J Biol Inorg Chem (2009) 14:253–260
DOI 10.1007/s00775-008-0445-9

ORIGINAL PAPER

Targeted Herceptin–dextran iron oxide nanoparticles for noninvasive imaging of HER2/neu receptors using MRI

Ting-Jung Chen · Tsan-Hwang Cheng · Chiao-Yun Chen · Sodio C. N. Hsu · Tian-Lu Cheng · Gin-Chung Liu · Yun-Ming Wang

Received: 1 August 2008 / Accepted: 14 October 2008 / Published online: 31 October 2008

Abstract A novel magnetic resonance imaging (MRI) contrast agent containing Herceptin is reported. The surfaces of superparamagnetic iron oxide nanoparticles were modified with dextran and conjugated with Herceptin (Herceptin–nanoparticles) to improve their dispersion, magnetization, and targeting of the specific receptors on cells. From analytical results, we found that Herceptin–nanoparticles were well dispersed in solutions of various pH range, and had no hysteresis, high saturation magnetization (80 emu/g), and low cytotoxicity to a variety of cells. Notably, the magnetic resonance enhancements for the different breast cancer cell lines (BT-474, SKBR-3, MDA-MB-231, and MCF-7) are proportional to the HER2/neu expression level in vitro. When Herceptin–nanoparticles were administered to mice bearing breast tumor allograft by intravenous injection, the tumor site was detected in T_2-weighted magnetic resonance images as a 45% enhancement drop, indicating a high level of accumulation of the contrast agent within the tumor sites. Therefore, targeting of cancer cells was observed by in vitro and in vivo MRI studies using Herceptin–nanoparticles contrast agent. In addition, Herceptin–nanoparticles enhancing the magnetic resonance signal intensity were sufficient to detect the cell lines with a low level of HER2/neu expression.

Keywords Superparamagnetic iron oxide · Herceptin · HER2/neu receptor · Magnetic resonance imaging

Introduction

Molecular imaging has recently been developed very rapidly and extensively in biotechnology. There is renewed interest in using superparamagnetic iron oxide (SPIO)

Electronic supplementary material The online version of this article (doi:10.1007/s00775-008-0445-9) contains supplementary material, which is available to authorized users.

T.-J. Chen · Y.-M. Wang (✉)
Department of Biological Science and Technology,
National Chiao Tung University,
75 Bo-Ai Street,
Hsinchu 300, Taiwan
e-mail: ymwang@mail.nctu.edu.tw

T.-H. Cheng
Department of Biological Science and Technology,
Chung Hwa University of Medical Technology,
89, Wunhua 1st Street, Rende,
Tainan County 717, Taiwan

C.-Y. Chen · G.-C. Liu
Department of Medical Imaging,
Kaohsiung Medical University Hospital,
Kaohsiung 807, Taiwan

C.-Y. Chen · G.-C. Liu
Department of Radiology,
Kaohsiung Medical University,
Kaohsiung 807, Taiwan

S. C. N. Hsu · Y.-M. Wang
Faculty of Medicinal and Applied Chemistry,
Kaohsiung Medical University,
100 Shih-Chuan 1st Road,
Kaohsiung 807, Taiwan

T.-L. Cheng
Faculty of Biomedical Science and Environmental Biology,
Kaohsiung Medical University,
100 Shih-Chuan 1st Road,
Kaohsiung 807, Taiwan

nanoparticles as multifunctional platforms for cell purifications in vitro, cellular and molecular imaging, and early (cellular-level) tumor diagnosis and treatments in vivo. SPIO nanoparticles with appropriate surface modification have been widely used for numerous in vivo applications, such as magnetic resonance imaging (MRI) contrast enhancement, immunoassay, detoxification of biological fluids, and drug delivery [1–4]. All these biomedical and bioengineering applications for MRI contrast media require that these nanoparticles have high magnetization and sizes smaller than 100 nm with an overall narrow particle size distribution. In addition, these applications require the magnetic particles to have special surface coatings, which achieve not only nontoxicity/biocompatibility but also allow targetable delivery in a specific area [5]. SPIO nanoparticles used in vitro or in vivo MRI are often coated with a polymer, which itself has frequently been used as a drug carrier because of its biocompatibility, water solubility, and ability to escape capture by macrophages [6–12]. These polymers include dextran, poly(ethylene glycol)s, and polyvinylpyrrolidone. To ensure the stability of the polymer coating in vivo, cross-linked iron oxide (CLIO) nanoparticles have been developed. CLIO nanoparticles are dextran-coated SPIO in which the dextran chains are chemically cross-linked [11].

Breast cancer is a common cancer among women worldwide, second only in frequency to skin cancer [13–16]. Some breast cancers (25–30%) begin in the lobules and the rest begin in other tissues [17]. Tumor-targeted drug delivery can improve the efficacy of chemotherapy while decreasing the systemic toxicity of these drugs. Trastuzumab (Herceptin) is a monoclonal antibody against HER2/neu that is currently used as a targeted therapy for some breast cancers. Between 15 and 25% of breast cancer patients are reported to respond to treatment with Herceptin [16] because of the high expression of HER2/neu receptors on the cancer cells in these patients [13–16, 18]. There are some reports indicating that macromolecules conjugated with Herceptin can recognize HER2/neu receptors and are internalized into cells via HER2/neu receptor-mediated endocytosis [19–22]. The usage and the mechanism of Herceptin have been reviewed extensively [13–16, 20], and these reports inspired us to test whether Herceptin conjugated to CLIO nanoparticles could be used for detecting breast cancer cells that overexpress HER2/neu receptors.

Recently, we reported folic acid conjugated with SPIO nanoparticles [23]. In this study, we synthesized a new T_2-weighted contrast agent in which SPIO nanoparticles were coated with dextran and conjugated to Herceptin (Herceptin–nanoparticles). The resulting nanoparticles were analyzed by thermal gravimetric analysis (TGA) and Fourier transform (FT) infrared (IR) spectroscopy. The geometric, structural, and physical properties of the Herceptin–nanoparticles contrast agent were characterized by transmission electron microscopy (TEM), dynamic light scattering (DLS), a 20-MHz relaxometer, and 3-T magnetic resonance imager. The magnetic properties of the nanoparticles were analyzed by a superconducting quantum interference measurement device (SQUID). Herceptin was immobilized on the surface of SPIO nanoparticles to increase the receptor-mediated internalization of Herceptin–nanoparticles in the targeted cancer cells and tumors. The cytotoxicity of Herceptin–nanoparticles to cancer cells was also investigated. In the in vitro imaging study, we used various amounts of HER2/neu expression receptors of breast cancer cell lines incubated with Herceptin–nanoparticles. In vivo MRI studies of tumor-bearing mice were also performed.

Materials and methods

Materials

All reagents used for the synthesis were purchased from commercial sources. These were ferric chloride hexahydrate ($FeCl_3{\cdot}6H_2O$), ferrous chloride tetrahydrate ($FeCl_2{\cdot}4H_2O$), and NH_4OH from Fluka; epichlorohydrin, 2,2′-(ethylenedioxy)bisethylamine (EDBE), 1-hydroxybenzotriazole, (benzotriazol-1-yloxy)tripyrrolidinophosphonium hexafluorophosphate, and paraformaldehyde from Sigma-Aldrich; dextran T-40, Sephacryl S-300, and Sephadex G-25 from GE Healthcare Bio-Sciences; Matrigel from BD Bioscience; and Spectrum molecular porous membrane tubing from Spectrum Laboratories. Antihuman IgG(γ-chain)–fluorescein isothiocyanate (FITC) and 4′,6-diamidino-2-phenylindole were purchased from Jackson ImmunoResearch.

Synthesis of SPIO

Dextran-coated magnetic iron oxide nanoparticles were prepared by mixing dextran T-40 [5 mL, 50% (w/w)] with an aqueous solution containing $FeCl_3{\cdot}6H_2O$ (0.45 g, 2.77 mmol) and $FeCl_2{\cdot}4H_2O$ (0.32 g, 2.52 mmol). The mixture was stirred vigorously at room temperature and NH_4OH [10 mL, 7.5% (v/v)] was rapidly added. The resulting black suspension was stirred continuously for 1 h and then centrifuged at 17,300*g* for 10 min to remove aggregate material. The SPIO nanoparticles were separated from unbound dextran T-40 by gel filtration chromatography on Sephacryl S-300. Five milliliters of the reaction mixture were applied to a 2.5 cm × 33 cm column and was eluted with a buffer solution containing 0.1 M sodium acetate and 0.15 M sodium chloride at pH 7.0. The purified dextran-coated magnetic iron oxide nanoparticles were

collected in the void volume. Column eluents were assayed for iron concentration at 330 nm by hydrochloric acid and for dextran at 490 nm by phenol/sulfuric acid [7]. IR (KBr) $\tilde{\nu} = 3{,}300$ (O–H), 2,800 (–CH_2– stretch).

Synthesis of CLIO

Five milliliters of SPIO nanoparticle solution at a concentration of 8 mg Fe/mL was added to a solution containing epichlorohydrin (3.3 mL, 35.66 mmol) and NaOH (5 M, 8.4 mL). After having been stirred vigorously for 24 h at room temperature, the product, CLIO, was dialyzed against 20 changes of distilled water in Spectrum molecular porous membrane tubing (12,000–14,000 cut off). IR (KBr) $\tilde{\nu} = 3{,}300$ (O–H).

Synthesis of CLIO–EDBE

CLIO and EDBE (1 mL, 6.7 μmol) in NaOH (5 M, 10 mL) were stirred for 24 h at room temperature. The solution was dialyzed against 20 changes of distilled water in Spectrum molecular porous membrane tubing (12,000–14,000 cut off). IR (KBr) $\tilde{\nu} = 3{,}300$–$3{,}400$, (O–H and –NH_2), 2,900 (–CH_2– stretch).

Synthesis of Herceptin–nanoparticles

One hundred microliters of the CLIO–EDBE at a concentration of 4 mg Fe/mL was added to 400 μL of Herceptin (Roche, Switzerland), using 1-hydroxybenzotriazole and (benzotriazol-1-yloxy)tripyrrolidinophosphonium hexafluorophosphate as catalysts, and the mixture was stirred for 24 h at room temperature. The solution was separated from unbound Herceptin by gel filtration chromatography on Sephadex G-25. Five milliliters of reaction mixture was applied to a 2.5 cm × 33 cm column and was eluted with phosphate-buffered saline (PBS). The amount of antibody was determined by UV spectrometry with background correction using a solution of Herceptin–nanoparticles of equal concentration with Warburg's formula: [14]

$$c\,(\mathrm{mg/mL}) = 1.55 \times (A_{280} - A_{320}) - 0.76 \times (A_{260} - A_{320}),$$

where c is the protein concentration calculated from the absorbance at the wavelengths indicated, and A is the absorbance.

Structural analysis

SQUID magnetometry measurements

Magnetic properties of SPIO were studied using a SQUID magnetometer, obtained from Quantum Design (XL-7 magnetic property measurement system), at fields ranging from −10 to 10 kOe and at 25 °C.

TEM measurements

The average core size, size distribution, and morphology were examined using a transmission electron microscope (JEOL JEM-2000 EX II, Japan) at a voltage of 100 kV. The composite dispersion was drop-cast onto a 200-mesh copper grid (Agar Scientific) and the grid was air-dried at room temperature before being loaded into the microscope.

Thermal gravimetric analysis

TGA (Setaram Labsys-TGDSC, Japan) is a simple analytical technique that measures the weight loss of a material as a function of temperature. The temperature of the sample gradually increased from 30 to 600 °C at a rate of 10 °C/min.

Relaxation time measurements

Relaxation times (T_1 and T_2) of an aqueous solution of Herceptin–nanoparticles were measured to determine relaxivity, r_1 and r_2. All measurements were made using a NMR relaxometer (NMS-120 Minispec, Bruker) operating at 20 MHz and 37.0 ± 0.1 °C. Before each measurement, the relaxometer was tuned and calibrated. The values of r_1 and r_2 were determined from eight data points generated by inversion recovery and a Carr–Purcell–Meiboom–Gill pulse sequence, respectively. Relaxation time measurements were also performed in a 3.0-T field in a clinical magnetic resonance scanner (Sigma; GE Medical Systems, Milwaukee, WI, USA). The following pulse sequences were used: (1) T_1-weighted sequence: echo time (TE) 150 ms, repetition time (TR) 100–2,000 ms; (2) T_2 weighted sequence: TR = 750 ms, TE = 50–300 ms. The field of view was set at 24 with ten excitations.

Cells and animal model

SKBR3, BT-474, MDA-MB-231, and MCF-7 cells are human breast cancer cells expressing HER2/neu receptors [11, 24]. KB cells, human nasopharyngeal epidermal carcinoma cell line, lack expression of HER2/neu receptors. All cells were obtained from the American Type Culture Collection (Manassas, VA, USA). SKBR3, BT-474, MDA-MB-231, and MCF-7 cells were cultured in McCoy's 5A medium (GIBCO), Hybri-care medium (American Type Culture Collection catalog no. 46-x) and supplemented with epidermal growth factor (Sigma; 30 ng/mL), Dulbecco's modified Eagle's medium (GIBCO), and L-15 medium (GIBCO), respectively. All media were

supplemented with 10% fetal bovine serum, sodium bicarbonate (1.5 g/L), sodium pyruvate (1.0 mM), and nonessential amino acid (0.1 mM). All cells were cultured at 37 °C in a humidified 5% CO_2 atmosphere.

BALB/cAnN.Cg-*Foxn1*^{nu}/CrlNarl mice (5 weeks old, female) and ICR mice (5 weeks old, female) were purchased from the National Laboratory Animal Center, Taipei, Taiwan. Animal experiments were performed in accordance with the institutional guidelines. SKBR-3 and KB cells in 100 μl (10^6 cells) PBS were injected subcutaneously into five nude mice . The cells were mixed in equal volume with Matrigel and injected into the right (KB) and left (SKBR-3) lateral thighs of the mice. An MRI experiment was performed 2 weeks after tumor implantation, at which time the tumors were measured to be at least 0.5 cm in diameter. This method produces a high yield of tumor in the lateral thighs of nude mice.

In vitro cell cytotoxicity analysis

All cell lines were used to measure the in vitro cell cytotoxicity of Herceptin–nanoparticles. An amount of 10^5 cells was plated in each well of the 96-well plates for 24 h. Then, Herceptin–nanoparticles were added at the desired concentrations (from 1 to 10 mM Fe per well). After 24 h of incubation, the supernatant was removed and the cells were washed three times with PBS. Cell viability was estimated using the 3-(4,5-dimethylthiazol-2-yl)-2,5-diphenyltetrazolium bromide (MTT) conversion test. Briefly, MTT (50 μl) solution was added to each well. After incubation for 2 h, each well was treated with dimethyl sulfoxide (50 μl) with pipetting. Absorption at 570 nm was measured on a plate reader. The data represent the average of four wells. Hundred percent viability was assumed from untreated cells.

In vitro specific targeting study

All cell lines were used to measure the in vitro specific targeting of Herceptin–nanoparticles. About 10^5 cells were plated in each well of the 24-well plates for 24 h. Then, Herceptin–nanoparticles were added at the predetermined concentrations (1 mM Fe per well). After 1 h of incubation at 4 °C, the supernatant was removed and the cells were washed three times with PBS. Then, the cells were incubated with antihuman IgG(γ-chain)–FITC for 1 h, washed using PBS three times, treated with paraformaldehyde (4%, 0.5 mL) solution for 10 min to fix the cells, and then washed with PBS. In addition, the nucleus was stained with 4′,6-diamidino-2-phenylindole (200 nM) solution for 3 min followed by washing with PBS three times and the cells were inspected using a confocal microscope.

In vitro MRI

MRI was performed with a clinical 3.0-T magnetic resonance scanner (Sigma; GE Medical Systems, Milwaukee, WI, USA) and a knee coil. All cell lines contained 2×10^6 cells and were incubated with Herceptin–nanoparticles (diluted in 1 mL medium, 0.3 mM Fe) for 30 min in an ice bath and then washed three times with PBS. All samples were scanned by a fast gradient echo pulse sequence (TR/TE/flip angel 3,000/90/10°).

In vivo MRI

Nude mice ($n = 5$) bearing SKBR-3 and KB tumors were studied by MRI when the subcutaneous tumor xenografts reached a diameter of 1.0 cm. A solution of Herceptin–nanoparticles (20 μmol/kg) was infused via the tail vein. The MRI of pentobarbital-anesthetized mice was performed at 0–3 h using a 3.0-T magnetic resonance scanner and a high-resolution animal coil (3.8-cm diameter). All animals were measured using a T_2-weighted fast spin-echo sequence (TR/TE 3,000/90, field of view 8) for imaging.

Biodistribution study in normal mice

Herceptin–nanoparticles (20 μmol/kg) were intravenously injected into groups of 18 male ICR mice. The mice were killed by ether at time intervals of blank, 15–90 min, and 24 h after the intravenous injection of Herceptin–nanoparticles (20 μmol/kg). Blood, brains, lungs, livers, spleens, and kidneys were collected and washed with 10 mL of PBS. The iron concentration of whole organs was measured by inductively coupled plasma mass spectrometry. The results were calculated as a percentage of injected dose per gram of tissue.

Results and discussion

In the work reported here, we modified the surface of SPIO so it would conjugate with Herceptin. The resulting nanoparticles were characterized by FT-IR spectroscopy, TEM, DLS, TGA, and SQUID magnetometry. Before Herceptin was conjugated to the SPIO, we premodified the surfaces of SPIO nanoparticles to improve the affinity of Herceptin conjugating to the particles. Scheme 1 shows a representation of the synthesis of Herceptin–nanoparticles. Initially, dextran immobilized on the SPIO nanoparticles was cross-linked by epichlorohydrin. Further, the CLIO nanoparticles were treated with EDBE to generate the primary amine functional group at the end of dextran. The resulting compounds of SPIO, CLIO, and CLIO–EDBE were confirmed by FT-IR spectroscopy (Fig. S1). Finally,

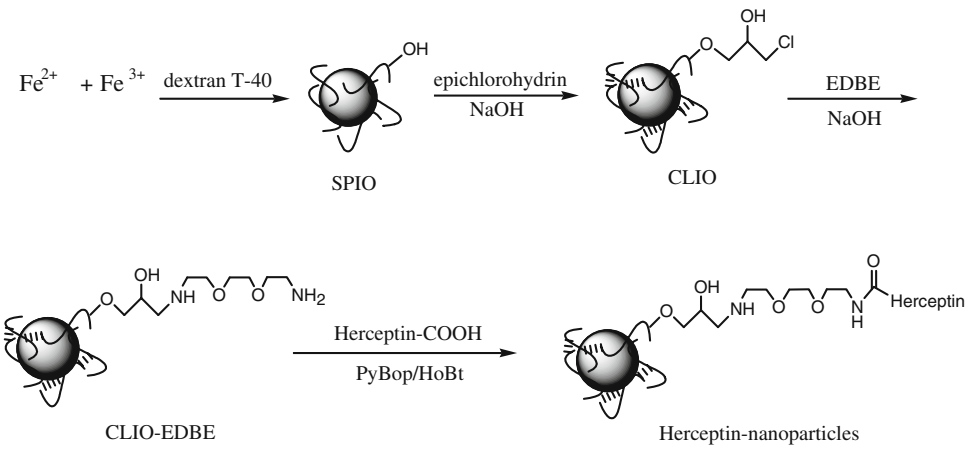

Scheme 1 The synthetic scheme of Herceptin–nanoparticles. *SPIO* superparamagnetic iron oxide, *CLIO* cross-linked iron oxide, *EDBE* 2,2′-(ethylenedioxy) bisethylamine, *PyBop* (benzotriazol-1-yloxy) tripyrrolidinophosphonium hexafluorophosphate, *HoBt* 1-hydroxybenzotriazole

Herceptin was conjugated with CLIO–EDBE in the presence of coupling agents. The formation of Herceptin–nanoparticles was confirmed by a bicinchoninic acid protein assay kit. Under the experimental conditions chosen, the Herceptin concentration was 5 mg/mL at 25 mM Fe. Figure 1 shows the TEM image of the Herceptin–nanoparticles. The TEM image indicates that the Herceptin–nanoparticles were well-dispersed. The core size of Herceptin–nanoparticles, calculated using 200 particles, was 3.5 ± 0.3 nm.

Typical size distributions of SPIO, CLIO, CLIO–EDBE, and Hercepin–nanoparticles were measured by DLS (Fig. S2). The DLS results show a slightly broad size distribution compared with the iron oxide nanoparticles synthesized in nonpolar solvents at high temperature [25–27]. According to the previous reports [7, 28], Herceptin–nanoparticles are not immediately removed from the circulation by the reticuloendothelial system, causing their small size, high biocompatibility, and water solubility.

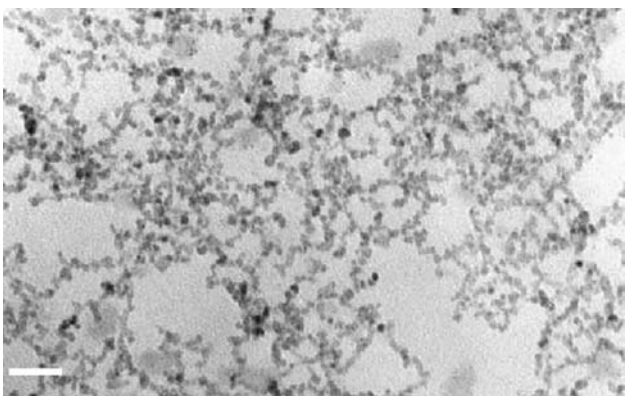

Fig. 1 Transmission electron microscopy image of Herceptin–nanoparticles. The average core size of Herceptin–nanoparticles is 3.5 ± 0.3 nm. *Bar* 20 nm

Further TGA was performed to confirm the coating formation and to estimate the efficiency of binding on the surface of SPIO [29]. The results indicated that thermograms of SPIO, CLIO, CLIO–EDBE, and Herceptin–nanoparticles were 40.6, 43.8, 48.0, and 61.2%, respectively (Fig. S3). According to the TGA results, the main weight loss was observed above 400 °C. It was confirmed that the iron oxide surfaces were coated with dextran, EDBE, and Herceptin.

A SQUID magnetometer was used to investigate the magnetic properties of Herceptin–nanoparticles. The magnetization of Herceptin–nanoparticles at 25 °C exhibited superparamagnetic behavior, i.e., high saturation magnetization (M_s) of 80 emu/g Fe and zero remanence on the magnetization loop (Fig. S4). It is noteworthy that the M_s value for Herceptin–nanoparticles in this work is much larger than those for other polymer-coated SPIO nanoparticles which possess approximately 30–50 emu/g Fe [5, 30–32]. A high-performance magnetic nanocrystal probe system has recently been developed for the diagnosis of breast cancer cells. The nanocrystal probes were synthesized through thermal decomposition of $Fe(acac)_3$ (acac is acetylacetonate) at high temperature in an organic solvent. The magnetization values of the nanocrystal probes in the reports [33, 34] are similar to that of our system.

In aqueous solution, the relaxivity values, r_1 and r_2, of the Herceptin–nanoparticles at 37.0 ± 0.1 °C and 20 MHz are 21 ± 1 and 144 ± 2 mM^{-1} s^{-1}, respectively, which are slightly lower than those of Resovist ($r_1 = 26$ and $r_2 = 164$ mM^{-1} s^{-1}) [35]. However, the r_1/r_2 ratio of Herceptin–nanoparticles is similar to that of Resovist. The r_1 and r_2 values of the Herceptin–nanoparticles at 3.0 T are 9.3 ± 1.1 and 200 ± 11 mM^{-1} s^{-1}, respectively.

To examine the stability of the Herceptin–nanoparticles under physiological conditions, the pH-dependent stability in the buffer solution was investigated (Fig. S5). Herceptin–nanoparticles were well dispersed in PBS (pH 7.4) as well as in the wide range of pH from 4 to 10 and did not display any aggregation for at least 4 months. We also used

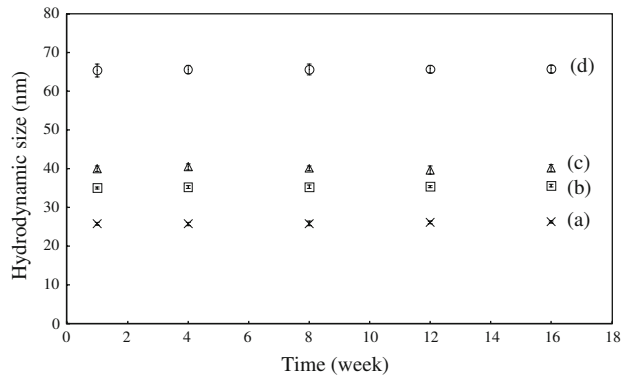

Fig. 2 Hydrodynamic size distribution with time of *a* superparamagnetic iron oxide, *b* cross-linked iron oxide (CLIO), *c* CLIO–2,2′-(ethylenedioxy)bisethylamine, and *d* Herceptin–nanoparticles

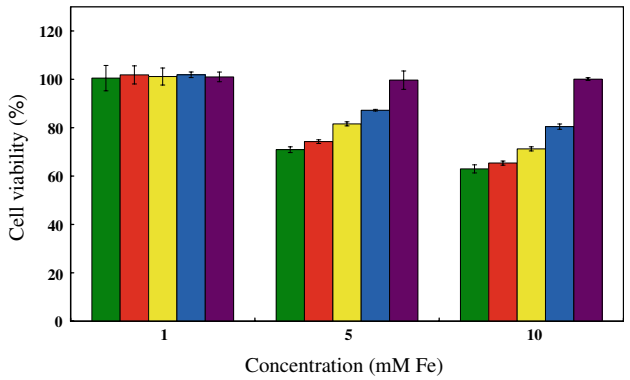

Fig. 3 In vitro cell viability of Herceptin–nanoparticles as a function of different iron concentrations in 3-(4,5-dimethylthiazole-2-yl)-2,5-diphenyltetrazolium bromide assay. *Green* BT-474 cell line, *red* SKBR-3 cell line, *yellow* MDA-MB-231 cell line, *blue* MCF-7 cell line, *purple* KB cell line

DLS to measure the long-term stability of the Herceptin–nanoparticles. The DLS results, as shown in Fig. 2, revealed that the nanoparticles did not aggregate in a period of 4 months. Further, the r_1 and r_2 values of Herceptin–nanoparticles were measured using a relaxometer at 20 MHz for 4 months after their synthesis. No significant change in their relaxivity values was observed (Fig. S6); thus, it has been demonstrated that Herceptin–nanoparticles are very stable.

The MTT assays using the BT-474, SKBR-3, MDA-MB-231, MCF-7, and KB cell lines were performed to analyze the potential cytotoxicity of Herceptin–nanoparticles. The results indicated that Herceptin–nanoparticles inhibited growth of cells that overexpress HER2/neu receptors (BT-474, SKBR-3, MDA-MB-231, and MCF-7) at high concentrations of iron (Fig. 3). However, Herceptin–nanoparticles were shown not to be cytotoxic at lower doses.

Targeting of Herceptin–nanoparticles was further examined using confocal microscopy and fluorescence imaging as shown in Fig. 4. After the incubation of Herceptin–nanoparticles with BT-474, SKBR-3, MDA-MB-231, MCF-7, and KB cell lines for 1 h at 4 °C, intracellular fluorescence was clearly observed in cultured HER2/neu overexpressing breast cancer cells in the presence of antihuman IgG(γ-chain)–FITC conjugated Herceptin–nanoparticles [15, 34]. It is well known that HER2/neu undergoes receptor-mediated endocytosis, which results in accumulation of the ligand–receptor complex inside the cells [36]. These imaging results are similar to that for polyamidoamine dendrimer generation five conjugated to anti-HER2 monoclonal antibody incubated with SKBR-3 cells [15].

The targeting of Herceptin–nanoparticles to HER2/neu receptor positive cells (BT-474, SKBR-3, MDA-MB-231, and MCF-7) was confirmed by in vitro MRI, as shown in Fig. 5. With the presence of the Herceptin–nanoparticles, the BT-474 and SKBR-3 cell lines, which have a relatively high HER2/neu expression level, showed noticeable magnetic resonance contrast. As the relative HER2/neu expression level increased, the enhancement of MRI increased proportionally. The enhancement follows Eq. 1:

$$\text{Enhancement } (\%) = \frac{\text{SI}_{\text{post}} - \text{SI}_{\text{pre}}}{\text{SI}_{\text{pre}}} \times 100\%, \quad (1)$$

where SI_{pre} is the signal intensity of cells not treated with the contrast agent and SI_{post} is the signal intensity of cells treated with the contrast agent. The negative enhancements for the BT-474, SKBR-3, MCF-7, and MDA-MB-231 cell lines were 75.4 ± 2.4, 70.9 ± 1.2, 40.8 ± 0.9, and $25.3 \pm 1.8\%$, respectively. The enhancements of positive cells in the presence of Herceptin–nanoparticles are significantly lower than those of positive cells in the absence

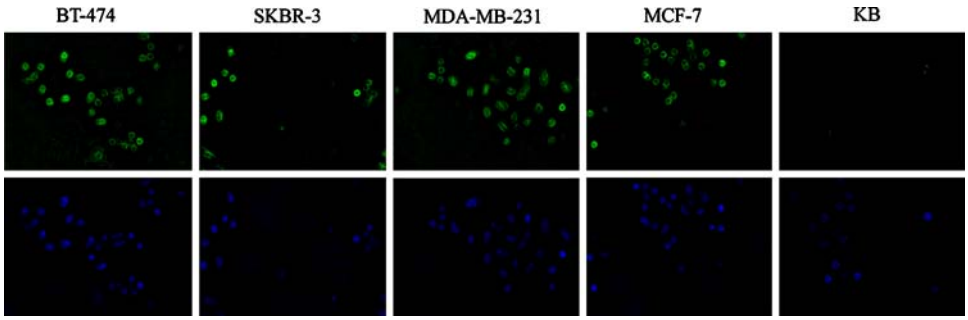

Fig. 4 The in vitro specific targeting study images. The *upper row* shows the cell lines incubated with Herceptin–nanoparticles (0.5 μmol/well) and treated with antihuman IgG–fluorescein isothiocyanate. The *lower row* shows the cell lines incubated with Herceptin–nanoparticles (0.5 μmol/well) and treated with 4′,6-diamidino-2-phenylindole

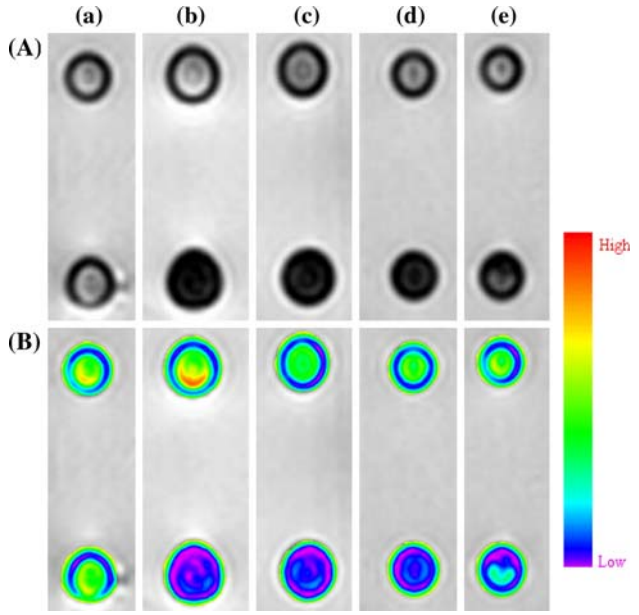

Fig. 5 T_2-weighted images of positive and negative cells for HER2/neu expression after the treatment with or without 0.3 mM Herceptin–nanoparticles. *a* KB cells, *b* BT-474 cells, *c* SKBR3 cells, *d* MDA-MB-231 cells, and *e* MCF-7 cells. The *upper rows* show cells without contrast agent treatment . The *lower rows* show cells treated with contrast agent. **A** Gray-level magnetic resonance imaging (MRI); **B** color-map MRI

of Herceptin–nanoparticles. No enhancement is observed for the negative cells (KB cells) in the presence or absence of Herceptin–nanoparticles. These results are consistent with those of previous report using magnetism-engineered iron oxide nanoparticles to detect breast cancer cells [37].

Tumor-bearing mice were prepared by subcutaneous injection of the SKBR-3 and KB cells into the left and right lateral thighs, respectively. MRI of the mice was performed at scheduled times after the intravenous injection of Herceptin–nanoparticles. Figure 6 shows the T_2-weighted fast spin echo images of a tumor-bearing mouse before (Fig. 6, left) and 1 h after (Fig. 6, right) the intravenous injection of Herceptin–nanoparticles. The enhancement of the SKBR-3 tumor is significantly lower than that of the KB tumor. The enhancement follows Eq. 2:

$$\text{Enhancement}\ (\%) = \frac{(\text{SI}_{\text{post}}/\text{SI}_{\text{p.post}}) - (\text{SI}_{\text{pre}}/\text{SI}_{\text{p.pre}})}{(\text{SI}_{\text{pre}}/\text{SI}_{\text{p.pre}})} \times 100\%, \quad (2)$$

where SI_{post} is the signal intensity of after injection, $\text{SI}_{\text{p.post}}$ is the signal intensity of the phantom after injection, SI_{pre} is the signal intensity before injection, and $\text{SI}_{\text{p.pre}}$ is the signal intensity of the phantom before injection. The region-of-interest analysis over the entire tumor indicates that the average enhancement decreased by about 45.7 ± 1.9 and $3.3 \pm 1.2\%$ for positive and negative tumors, respectively. In other words, the Herceptin–nanoparticles have

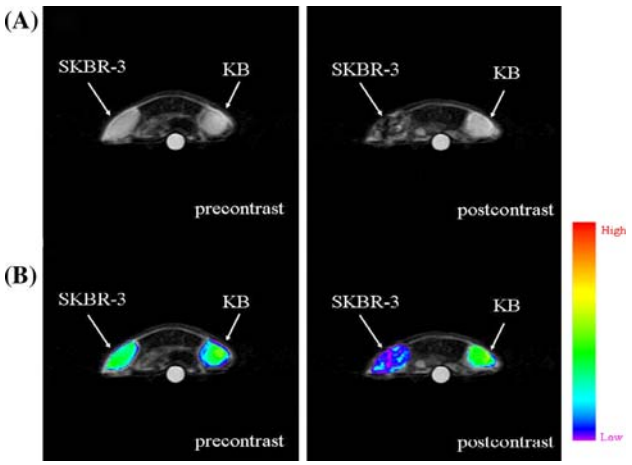

Fig. 6 T_2-weighted images before and after injection of Herceptin–nanoparticles. **A** gray-level MRI; **B** color-map MRI

specifically targeted the HER2/neu receptor-expressing tumors. In addition, the enhancement drop of MRI for Herceptin–nanoparticles is also consistent with that of iron oxide nanoparticles doped with Mn(II) ions that are conjugated with Herceptin and injected into tumor-bearing nude mice [37]. Specific targeting of a contrast agent can result in a lower dose being required to obtain a diagnostic response. Hence, our results indicate that Herceptin–nanoparticles accumulate to a detectable amount in tumors expressed with the HER2/neu receptor.

A biodistribution study was performed with Herceptin–nanoparticles using inductively coupled plasma mass spectrometry analyses. The results obtained from this study should be useful for better understanding the tissue targeting of Herceptin–nanoparticles (Fig. S7). The biodistribution in organs or tissues was compared in the presence and in the absence of Herceptin–nanoparticles. The iron concentration in blood increased after injection of the Herceptin–nanoparticles and then slowly declined thereafter (24 h). Significant changes in iron concentration were observed from tissue to tissue. The iron level in the heart and lung peaked at about 30 min, and then gradually declined over 24 h. Other tissues, such as liver and spleen, showed steady increases of the iron levels about 15 min after injection of Herceptin–nanoparticles, but the iron level in brain was not affected.

Conclusion

We have successfully prepared and characterized biocompatible superparamagnetic Herceptin–nanoparticles. They are hydrophilic, weakly cell cytotoxic, and well dispersed under physiological conditions. Moreover, Herceptin–nanoparticles have the ability to target and differentiate

human breast cancer cells with different HER2/neu expression levels such as BT-474, SKBR-3, MDA-MB-231, and MCF-7 and tumors as proven by in vitro and in vivo MRI studies. Therefore, Herceptin–nanoparticles can be potentially used as an MRI contrast agent for the detection of HER2/neu-expressing breast cancer.

Acknowledgements We are grateful to the National Science Council of the Republic of China for financial support under contracts no. NSC 96-2627-M-037-001 and NSC 97-2623-7-037-001-NU. This research was also supported in part by grants from National Health Research Institutes under contract no. NHRI-EX-95-9424EI.

References

1. Sun C, Veiseh O, Gunn J, Fang C, Hansen S, Lee D, Sze R, Ellenbogen RG, Olson J, Zhang M (2008) Small 4:240–249
2. Schellenberger E, Schnorr J, Reutelingsperger C, Ungethüm L, Meyer W, Taupitz M, Hamm B (2008) Small 4:225–230
3. Li Z, Tan B, Allix M, Cooper AI, Rosseinsky MJ (2008) Small 4:231–239
4. Kalambur VS, Longmire EK, Bischof JC (2007) Langmuir 23:12329–12336
5. Gupta AK, Gupta M (2005) Biomaterials 26:3995–4021
6. Yigit MV, Mazumdar D, Kim H-K, Lee JH, Odintsov B, Lu Y (2007) Chembiochem 8:1675–1678
7. Paul KG, Frigo TB, Groman JY, Groman EV (2004) Bioconjug Chem 15:194–401
8. Koch AM, Reynolds F, Kircher MF, Merkle HP, Weissleder R, Josephson L (2003) Bioconjug Chem 14:1115–1121
9. Josephson L, Kircher MF, Mahmood U, Tang Y, Weissleder R (2002) Bioconjug Chem 13:554–560
10. Högemann D, Josephson L, Weissleder R, Basilion JP (2000) Bioconjug Chem 11:941–946
11. Lee H, Yu MK, Park S, Moon S, Min JJ, Jeong YY, Kang H-W, Jon S (2007) J. Am Chem Soc 129:12739–12745
12. Choi H, Choi SR, Zhou R, Kung HF, Chen IW (2004) Acad Radiol 11:996–1004
13. Tran T, Engfeldt T, Orlova A, Sandström M, Feldwisch J, Abrahmsén L, Wennborg A, Tolmachev V, Karlström AE (2007) Bioconjug Chem 18:1956–1964
14. Germershaus O, Merdan T, Bakowsky U, Behe M, Kissel T (2006) Bioconjug Chem 17:1190–1199
15. Shukla R, Thomas TP, Peters JL, Desai AM, Kukowska-Latallo J, Patri AK, Kotlyar A, Baker JR (2006) Bioconjug Chem 17:1109–1115
16. Hilger I, Leistner Y, Berndt A, Fritsche C, Haas KM, Kosmehl H, Kaiser WA (2004) Eur Radiol 14:1124–1129
17. Pan M-H, Lin C-C, Lin J-K, Chen W-J (2007) J Agric Food Chem 55:5030–5037
18. Suna B, Ranganathana B, Feng S-S (2008) Biomaterials 29:475–486
19. Bergman I, Whitaker-Dowling P, Gao Y, Griffin JA, Watkinse SC (2003) Virology 316:337–347
20. Colbern GT, Hiller AJ, Musterer RS, Working PK, Henderson IC (1999) J Inorg Biochem 77:117–120
21. Meares CF, Chmura AJ, Orton MS, Corneillie TM, Awhetstone P (2003) J Mol Recognit 16:255–259
22. Garmestania K, Milenica DE, Plascjakb PS, Brechbiel MW (2002) Nucl Med Biol 29:599–606
23. Chen T-J, Cheng T-H, Hung Y-C, Lin K-T, Liuc G-C, Wang Y-M (2008) J Biomed Mater Res A 87:165–175
24. Taktak S, Sosnovik D, Cima MJ, Weissleder R, Josephson L (2007) Anal Chem 79:8863–8869
25. Casula MF, Y-w Jun, Zaziski DJ, Chan EM, Corrias A, Alivisatos AP (2006) J Am Chem Soc 128:1675–1682
26. Park J, Lee E, Hwang N-M, Kang M, Kim SC, Hwang Y, Park J-G, Noh H-J, Kim J-Y, Park J-H, Hyeon T (2005) Angew Chem Int Ed 44:2872–2877
27. Sun S, Zeng H (2002) J Am Chem Soc 124:8204–8205
28. Weissleder R, Elizondo G, Wittenberg J, Rabito CA, Bengele HH, Josephson L (1990) Radiology 175:485–493
29. Lee H, Lee E, Kim DK, Jang NK, Jeong YY, Jon S (2006) J Am Chem Soc 128:7383–7389
30. Cheng F-Y, Su C-H, Yang Y-S, Yeh C-S, Tsai C-Y, Wu C-L, Wu M-T, Shieh D-B (2005) Biomaterials 26:729–738
31. Shieh D-B, Cheng F-Y, Su C-H, Yeh C-S, Wu M-T, Wu Y-N, Tsai C-Y, Wu C-L, Chen D-H, Chou C-H (2005) Biomaterials 26:7183–7191
32. Varanda LC, Jafelicci M, Tartaj P, O'Grady K, González-Carreño T, Morales MP, Muñoz T, Serna CJ (2002) J Appl Phys 92:2079–2085
33. Jun Y-W, Huh Y-M, Choi J-S, Lee J-H, Song H-T, Kim S, Yoon S, Kim K-S, Shin J-S, Suh J-S, Cheon J (2005) J Am Chem Soc 127:5732–5733
34. Huh Y-M, Jun Y-W, Song H-T, Kim S, Choi J-S, Lee J-H, Yoon S, Kim K-S, Shin J-S, Suh J-S, Cheon J (2005) J Am Chem Soc 127:12387–12391
35. Horák D, Babič M, Jendelová P, Herynek V, Trchova M, Pientka Z, Pollert E, Hájek M, Syková E (2007) Bioconjug Chem 8:635–644
36. Sturla SJ, Irwin JJ, Loeppky RN, Mulvihill MJ, Searcey M (2007) ACS Chem Biol 2:286–292
37. Lee J-H, Huh Y-M, Jun Y-W, Seo J-W, Jang J-T, Song H-T, Kim S, Cho E-J, Yoon H-G, Suh J-S, Cheon J (2006) Nat Med 13:95–99